Dynamics of methyl radical formation by 266 nm photolysis of xylenes and mesitylene

Namitha Brijit Bejoy, Monali Kawade, Sumitra Singh and G. Naresh Patwari*

Department of Chemistry, Indian Institute of Technology Bombay, Powai, Mumbai 400076, India

E-mail: naresh@chem.iitb.ac.in

ABSTRACT

The 266 nm photodissociation of three xylene isomers and mesitylene leading to the formation of methyl radical was examined. The kinetic energy release profiles for the methyl radical were almost identical for all the three isomers of xylene and mesitylene, while substantial differences were observed for the corresponding profiles of the co-fragment produced by loss of one methyl group. This observation be attributed to the formation of the methyl radical from alternate channels. The total kinetic energy distribution profiles were rationalized based on the dissociation of {sp^2}C–C{sp^3} bond in the cationic state, wherein the {sp^2}C–C{sp^3} bond dissociation energy is lowered relative to the ground state.

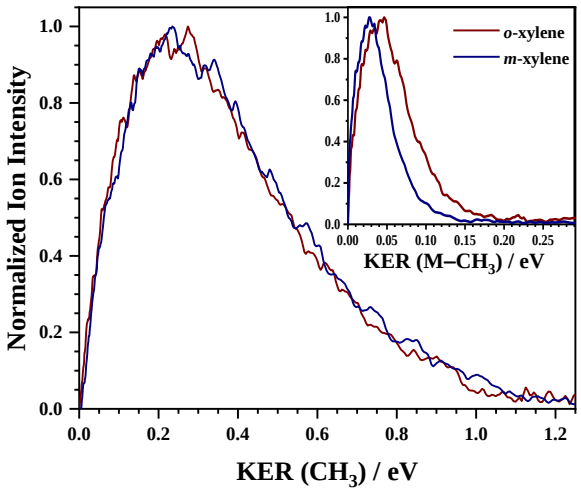

The dissocaiton in the cationic state follows a resonant three-photon absorption process, resulting in maximum total kinetic energy of about 1.6 – 1.8 eV for the photofragments. A results in. Fitting of the TKER distribution profiles to empirical function reveals that the dynamics of {sp^2}C–C{sp^3} bond dissociation is insensitive to the position of substitution but marginally dependent on the number of methyl groups.

INTRODUCTION

Benzene and its derivatives are prototypical molecules used frequently for studying photodissociation dynamics,[1–6] as they serve as building blocks of complex (bio)molecules and various factors such as the presence of the aromatic chromophore, type and position of the substitution influences the photophysical properties of these molecules. Alkylbenzenes such as toluene and xylenes have very important applications in combustion chemistry as anti-knock agents.[7,8] Even though the electronic structure of alkylbenzenes is similar to that of benzene owing to the π electron structure, the substitution of the methyl group changes the symmetry of the states and selection rules, thereby altering the photophysics and photochemistry, in comparison to benzene.[9,10] In case of benzene, a single photon absorption in the range of 190 to 270 nm leads to several radiative and non-radiative decay processes such as photodissociation and isomerization.[2] Photodissociation in case of toluene and xylene results primarily in the α-H atom elimination, which leads to the formation of benzyl radical either by direct dissociation from the excited state or indirect dissociation after internal conversion to the vibrationally hot ground state[3,11–13] The presence of the aromatic chromophore increases the probability of multiphoton absorption which enables the molecules to access the ground and excited states of the cation.[14–16] Earlier experiments on the dynamics of methylbenzene cations have been investigated mostly using photoelectron spectroscopy. In the case of 1,3,5-cycloheptatriene and toluene, only the H-atom loss channel opens up during dissociative photoionization, leading to the formation of tropylium and benzyl cations.[17] On the other hand, the loss of methyl fragment is a prominent product channel in the case of xylenes.[18–20] However, reports on direct detection of methyl fragment following the photodissociation of methyl substituted benzene are sparse and especially, the 266 nm photolysis of alkylbenzenes in the gas-phase is conspicuously missing in the literature. In xylenes and mesitylene the {sp^2}C–C{sp^3} bond dissociation (around 4.50 eV)[21] and the $S_0 \longrightarrow S_1$ excitation (around 4.60 eV)[22,23] energies are marginally lower than the 266 nm (4.66 eV) excitation energy. This leads to an interesting scenario of competing pathways in the molecules and provides motivation to investigate 266 nm photodissociation of methyl benzenes using velocity map imaging technique. Along with this, effect of the position of

methyl substitution on the aromatic ring and the effect of the number of methyl substitutions on photodissociation dynamics has also been explored in this work.

METHODOLOGY

The setup for carrying out velocity map imaging experiments is described elsewhere.[24] Briefly, a skimmed molecular beam of helium (3 atm) doped with the desired reagent (*o*-xylene, *m*-xylene, *p*-xylene, or mesitylene; Sigma Aldrich) was intersected by counter-propagating pump (266 nm) and probe (333.45 nm) lasers. The ensuing cations were imaged using a four-electrode velocity map imaging (VMI) spectrometer fitted with a 50 mm diameter two-stage microchannel plate (MCP) and a P47 phosphor screen (MCP-50DLP47VF; Tectra). In the time-of-flight (TOF) mode, the front-plate of the MCP is grounded, the back-plate and the phosphor screen are held around +1500 V and an RC circuit was used to extract the signal which is processed with a 350 MHz preamplifier (SR445A; Stanford Research Systems). In the imaging mode, the front-plate of the MCP detector is gated with a 75 ns pulse of –1000 V (HTS 40-06-OT-75; Behlke), while the back-plate and the phosphor are held at +800 and +3000 V, respectively. The gate time of the front plate is adjusted to match the arrival time of the desired ion. The image on the phosphor screen was recorded with a high-performance, easy-to-use USB, GigE CMOS camera (IDS Imaging Development Systems) and the raw images were acquired using NuAcq software[25] with 50,000 shots. The aquired images were further processed (symmetrized) using ImageJ software[26] and Abel inversion was carried out by the Basis Set Expansion method (BASEX) to extract the kinetic energy spectrum.[27] In the present set of experiments the pump laser (266 nm) is the fourth harmonic of an Nd: YAG laser (Brilliant-B; Quantel) and the probe laser (333.45 nm) is the frequency-doubled output of a tunable dye laser (LiopStar-HQ; LIOP-TEK) pumped with the second harmonic of an Nd: YAG laser (Brilliant-B; Quantel). The plane of polarization of both the lasers is kept parallel to the plane of the detector. The delay between the pump and probe lasers is approximately 10 ns. The timings for the opening of the pulsed nozzle, the firing of the two lasers (both flashlamp and Q-switch triggers), gating the front-plate of the MCP detector, and the opening of the camera shutter were electronically controlled with an 8-channel digital delay pulse generator (DDG-9520; Quantum

Composers). The energy of the pump and the probe lasers were kept around 1 mJ/pulse and 500 μJ/pulse, respectively. The laser flux was optimized such that signal intensity was negligible for the methyl fragment in the absence of probe laser.

RESULTS and DISCUSSION

The mass spectra presented in Figure 1, following 266 nm photolysis of three xylene isomers and mesitylene, show intense peaks corresponding to the molecular ion peak at 106 $[C_6H_4(CH_3)_2]^+$ and 120 $[C_6H_4(CH_3)_3]^+$ amu, respectively. Further, extensive fragmentation leading to the appearance of C_nH_m (n=2-6) can be seen in almost all the cases, except for *m*-xylene, wherein the fragmentation appears to be less efficient. However, in all the other cases the loss of one methyl group is the dominant fragmentation pathway. This loss of the methyl fragment was probed using the well-known 2+1 REMPI method with 333.45 nm excitation of its ground (ν=0) state,[28] and the resulting pump-probe mass spectra (shown as green-traces in Figure 1) show the appearance of the methyl fragment at 15 amu. Comparison of the pump-only mass spectra (red-traces in Figure 1) with the pump-probe mass spectra (green-traces in Figure 1), in general, suggests that the probe laser enhances the intensity of the C_nH_m (n=1-4) fragments, while lowering the intensity corresponding to n=5, 6 fragments,[29] except for *m*-xylene, wherein all the signals, including the parent ion, increase in the presence of probe laser. In the case of *p*-xylene, *o*-xylene, and mesitylene the lowering of the peak intensity for the loss of one methyl group (91 and 105 amu, respectively) can probably be attributed to the probe laser induced fragmentation of the vibrationally hot $[C_6H_4(CH_3)_2]$/$[C_6H_4(CH_3)_3]$ cations. Whereas, in the case of *m*-xylene, the enhancement of the corresponding signal could be attributed to the predissociation mediated by accidental resonance with the probe laser frequency.

The velocity map images of the methyl fragment and the corresponding co-fragment (co-fragment, hereon means the fragment produced by loss of one methyl group from the parent molecule) were collected by appropriately time gating the front plate of the detector and are shown in Figure 2 for all the three xylene isomers and mesitylene. The ion-images for the CH_3 (methyl) fragment were obtained in the pump-probe configuration, while those of the co-fragment were acquired with the pump-only configuration. The co-fragment image

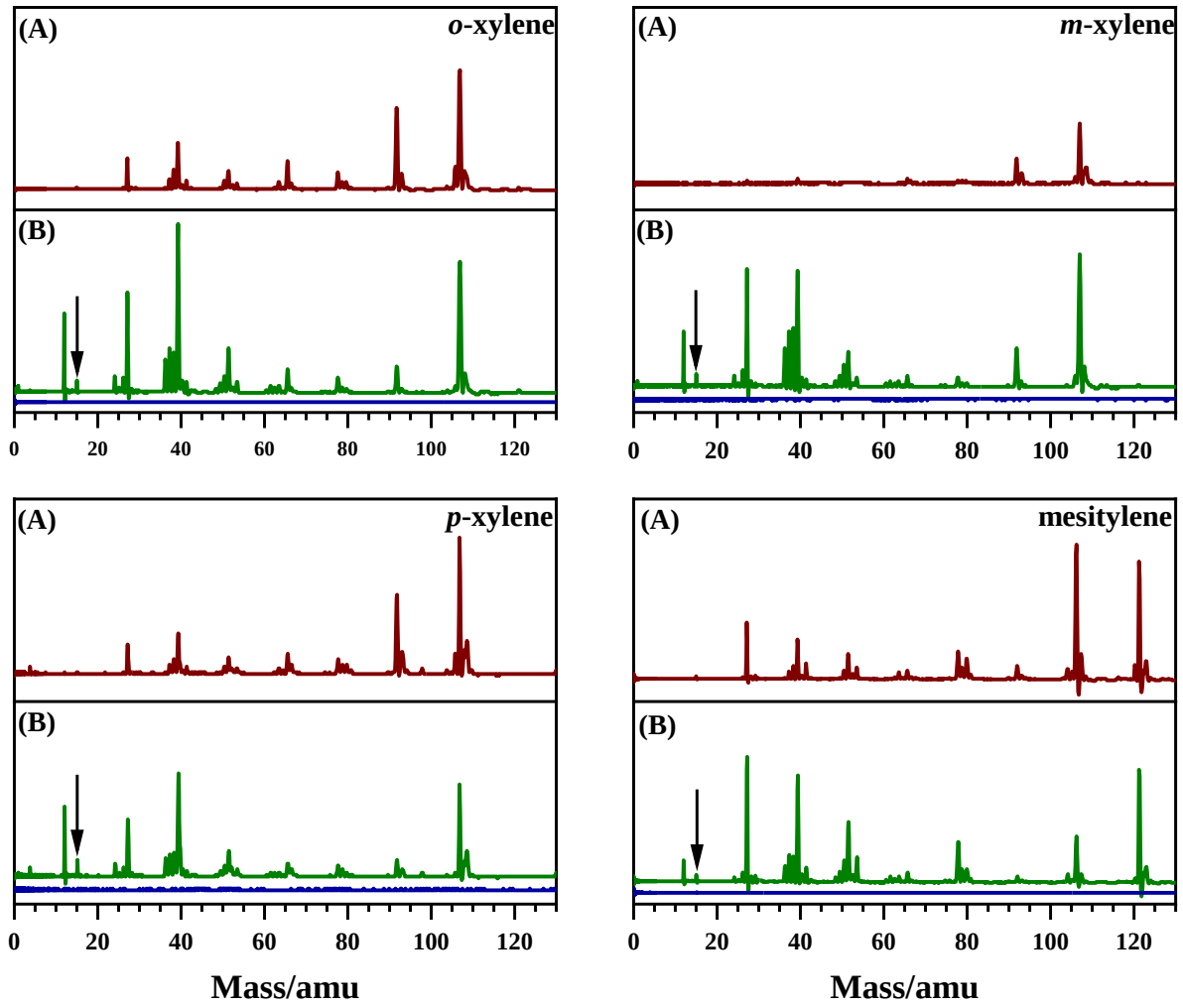

Figure 1. (A) The pump-only mass spectra following 266 nm photolysis (red-trace) and (B) the pump-probe mass spectra following 266 nm photolysis and 333.45 nm probe, resulting in 2+1 REMPI of the methyl fragment (green-trace). The methyl fragment $[CH_3]^+$ signal at 15 amu is indicated by the black arrow, appears only in the presence of both the pump and the probe lasers. No ion signal was observed in the presence of only the probe laser (blue-trace). All the spectra were recorded at the same pump laser power.

shows significant intensity close to the center indicating that these cations have near-zero kinetic energy. In comparison, the velocity map images of methyl fragment are more diffused and exhibit a central blob-like feature indicating a broader kinetic energy distribution.[24] The isotropic nature of the images can be attributed to{sp^2}C-C{sp^3} bond cleavage via pre-dissociation pathway, which has a longer time scale than rotational reorientation time,[30] unlike the case of methyl iodide or dimethyl sulfide.[31,32] The KER (Kinetic Energy Release)

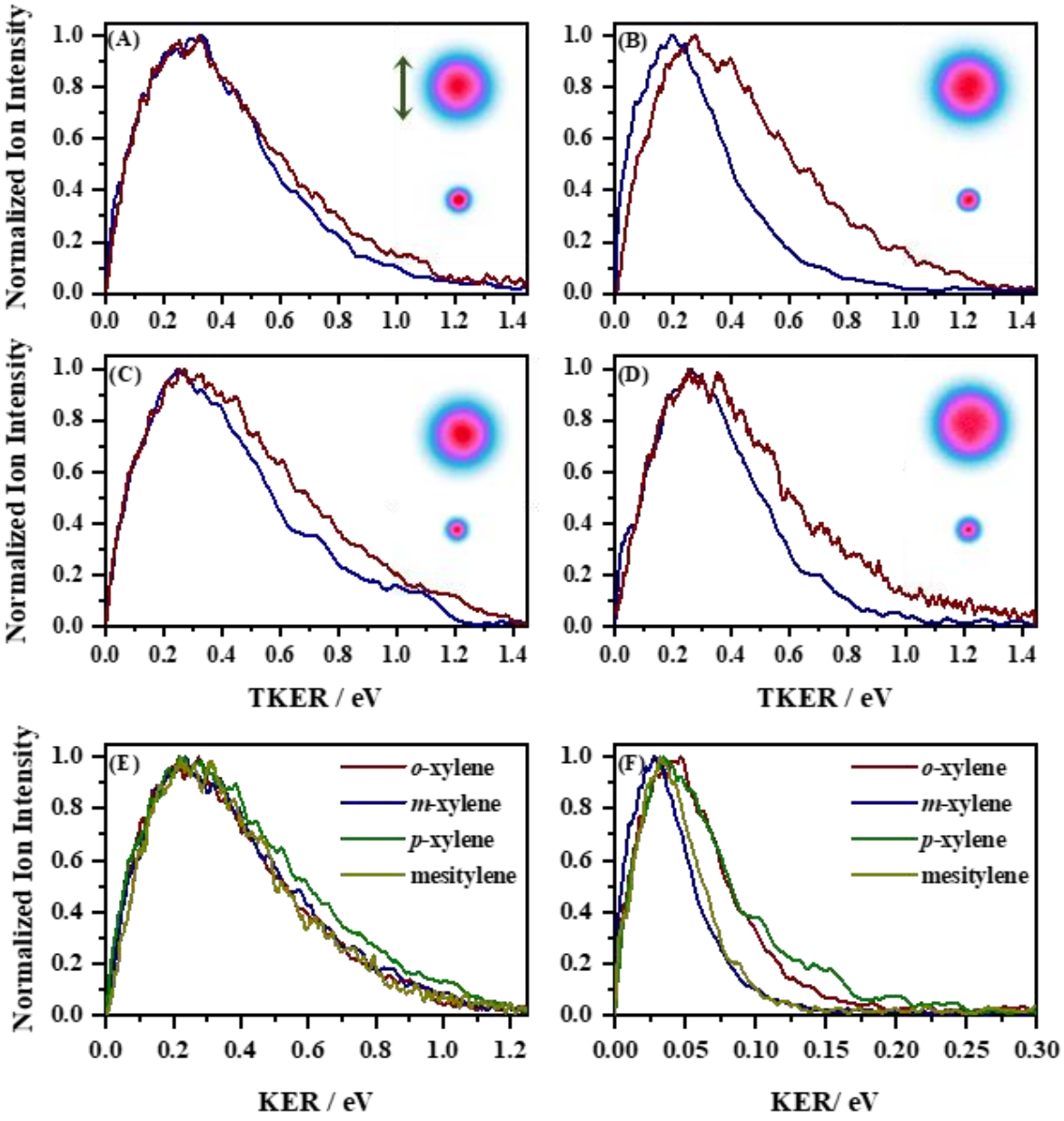

Figure 2. Normalized total kinetic energy release (TKER) distribution plots for (A) *o*-xylene, (B) *m*-xylene, (C) *p*-xylene and (D) mesitylene (D). In each case the red and blue curves represent the TKER plots of the methyl radical and the co-fragment originating from loss of methyl group from the parent molecule, respectively. Symmetrized velocity map images of methyl group (top) and the co-fragment (bottom) are shown in each case. All the images are on the same scale and the arrow in the first image frame shows the direction of laser polarization. Normalized kinetic energy release (KER) distribution plots for (E) methyl group and (F) co-fragment for all four compounds. All images were recorded using the same pump laser power. All experiments were carried out at least three times and representative results are shown.

TABLE 1: Area under the TKER (Figure 2) and KER (Figure 2) profiles for the methyl fragment and its corresponding co-fragment. R is the ratio of values of ∫(TKER) for the methyl fragment and its corresponding co-fragment.

	Methyl fragment		Co-fragment		
	∫(KER)	∫(TKER)	∫(KER)	∫(TKER)	R
o-xylene	0.50	0.60	0.081	0.56	1.07
m-xylene	0.51	0.59	0.058	0.40	1.48
p-xylene	0.57	0.66	0.088	0.56	1.17
mesitylene	0.49	0.59	0.059	0.45	1.29

and TKER (Total Kinetic Energy Release) distributions, shown in Figure 2, were extracted from the corresponding images. The integrals (area under the curves) of KER and TKER distribution curves are listed in Table 1. The comparison of the TKER distribution curves (and the corresponding integrals) of the methyl group and the co-fragment reveals that the two TKER profiles are not identical within the experimental uncertainty, with the exception of *o*-xylene for which the ratio of area under the TKER profiles (R) is 1.07, a value very close to unity. The difference in the TKER profiles is largest in the case of *m*-xylene (R=1.48) followed by mesitylene (R=1.29) and p-xylene (R=1.17). In order to understand this observation, the KER profiles of the methyl and the co-fragment were examined in all the cases (Figure 2E and 2F). The KER profiles of the methyl group (and the corresponding integrals) indicates that the formation of the methyl group in the ν=0 state is identical for *o*-xylene, *m*-xylene and mesitylene, while *p*-xylene is marginally different. On the other hand, the KER profiles for the co-fragment can be broadly classified into two sets, one from *o*-xylene and *p*-xylene and the other from *m*-xylene and mesitylene, with a substantial difference in the KER profiles. The KER profiles of *m*-xylene and mesitylene co-fragments show much narrower KER distribution in comparison with *o*-xylene and *p*-xylene co-fragments, which is also reflected in the corresponding KER integrals (see Table 1). These results suggest that the dynamics of co-fragment formation are different for the two sets (*o*-xylene and *p*-xylene versus *m*-xylene and mesitylene). Therefore, in the case of *m*-xylene and mesitylene the differences in the TKER profiles of the methyl group and the co-fragment are attributed to

probe induced dissociation following pump excitation of the parent molecule and/or probe induced sequential dissociation (loss methyl group from hot neutral co-fragment).[29] The mismatch in the TKER plots (see Figure 2B) is more pronounced in the case of *m*-xylene, and the peak is shifted to lower energy in comparison with other co-fragments (see Figure 2F) as a result of probe induced fragmentation due to 'accidental resonance'. Further, experiments on xylyl radicals have shown a difference for the *m*-xylyl radicals compared to the other isomers. The largest change in geometry occurs in meta substitution, which facilitates the faster deactivation owing access to several conical intersections.[33] Further, the absorption of the probe laser photon by the parent molecular cation could lead to direct dissociation, which can contribute to lowering of the kinetic energy distribution, as seen in the case of *m*-xylene.

The generalized energy level scheme for the formation of CH_3 radicals in all four compounds is shown in Figure 3. The values corresponding to bond dissociation energies in the neutral and cationic ground states were calculated using the G3B3[34] method with Gaussian-16,[35] experimentally measured ionization energies[22,36] and $S_0 \longrightarrow S_1$ transition energies[22,23] are listed in Table 2. In xylenes and mesitylene the {sp^2}C–C{sp^3} bond dissociation energy in the neutral ground state [BDE(S_0), see Table 2] is about 0.2 eV lower than the 266 nm (4.66 eV) photon energy. Thus, {sp^2}C–C{sp^3} dissociation in the S_0 state would result in TKER of about 0.2 eV, which is much lower than the experimentally observed value (see Figure 2). In all the four compounds, the $S_0 \longrightarrow S_1$ transition energy is marginally less than 4.66 (266 nm), therefore absorption of the first 266 nm photon results in vibrionic excitation just above the band-origin (0_0^0) of the S_1 state, which serves as a resonant intermediate level for the subsequent absorption of the second 266 nm photon leading to ionization, which however, will not result in the {sp^2}C–C{sp^3} dissociation. Absorption of the third photon excites the parent molecule above the {sp^2}C–C{sp^3} bond dissociation energy in the cationic ground state [BDE(D_0), see Table 2], resulting in excess energy, which is termed as E_T^{max}, and in the present scenario based on the energy level scheme shown in Figure 3, the value of E_T^{max} can be calculated using equation (1).

$$E_T^{max} = 3 * 4.66 - IE - BDE(D_0) \text{ in eV} \qquad (1)$$

The calculated E_T^{max} values are also listed in Table 2 and range from 1.62 to 1.77 eV.

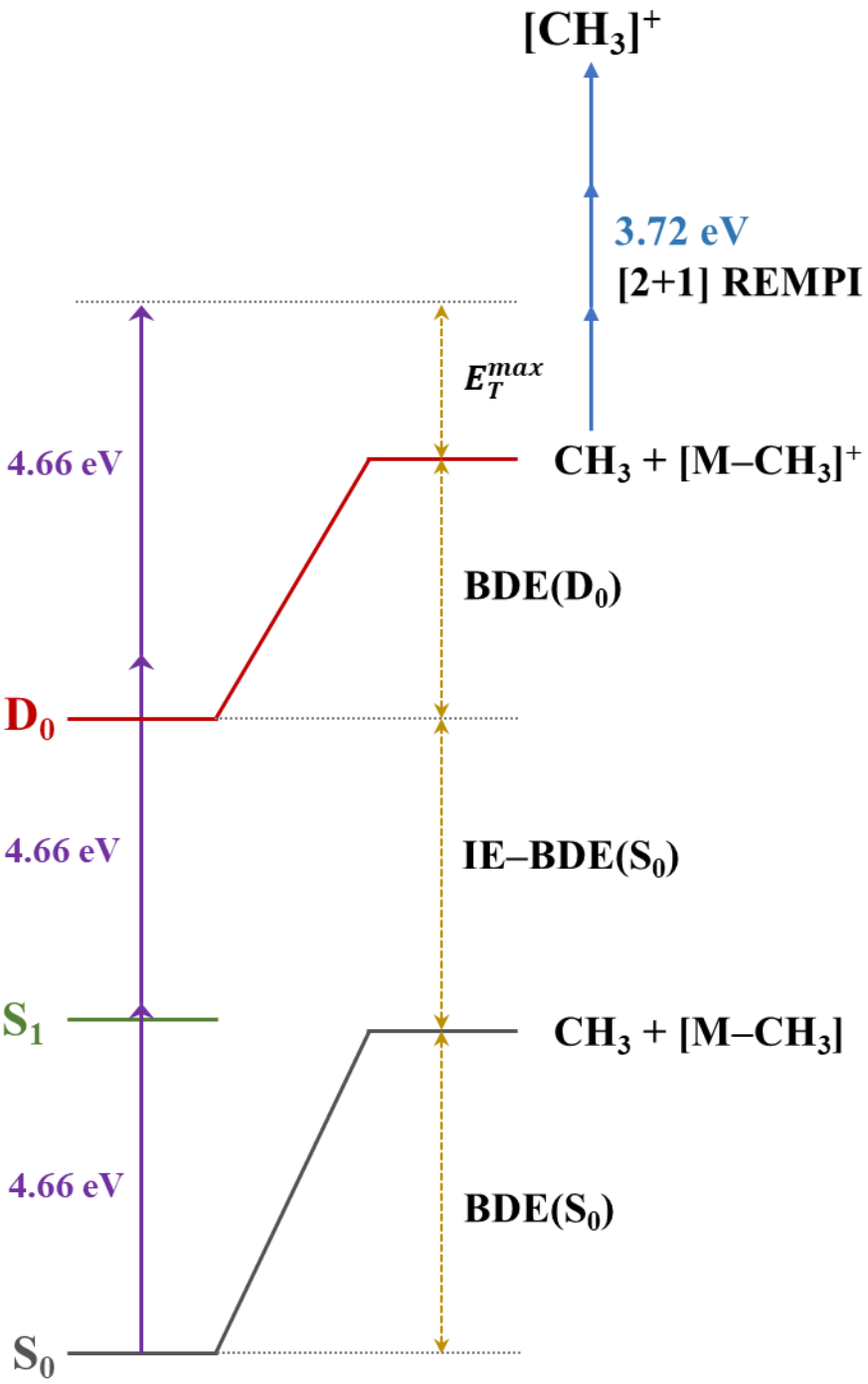

Figure 3. Generalized schematic of the energy level scheme for the {sp^2}C–C{sp^3} bond dissociation for methyl benzenes in various states. The terms used are as follows:S_0: neutral ground state; S_1: first excited state; D_0: cationic ground state; BDE(S_0): {sp^2}C–C{sp^3} bond dissociation energy in the S_0 state; CH_3: methyl fragment; [M–CH_3]: co-fragment obtained by loss of one methyl group from parent molecule; BDE(D_0): {sp^2}C–C{sp^3} bond dissociation energy in the D_0 state; IE: ionization energy; E_T^{max}: maximum translational energy (in the center-of-mass frame).

TABLE 2: Energies (eV) for various (excitation) process shown in the energy level schematic (Figure 3).

	$BDE(S_0)^a$	$BDE(D_0)^a$	$S_0 \rightarrow S_1$	IE	E_T^{max}
o-xylene	4.46^a	3.77^a	4.63^b	8.58^b	1.63
m-xylene	4.47^a	3.79^a	4.58^b	8.57^b	1.62
p-xylene	4.46^a	3.89^a	4.55^b	8.45^b	1.64
mesitylene	4.47^a	3.80^a	4.52^c	8.41^d	1.77

[a]This work, calculated using G3B3 method; [b]Ref [22]; [c]Ref [23]; [b]Ref [36]

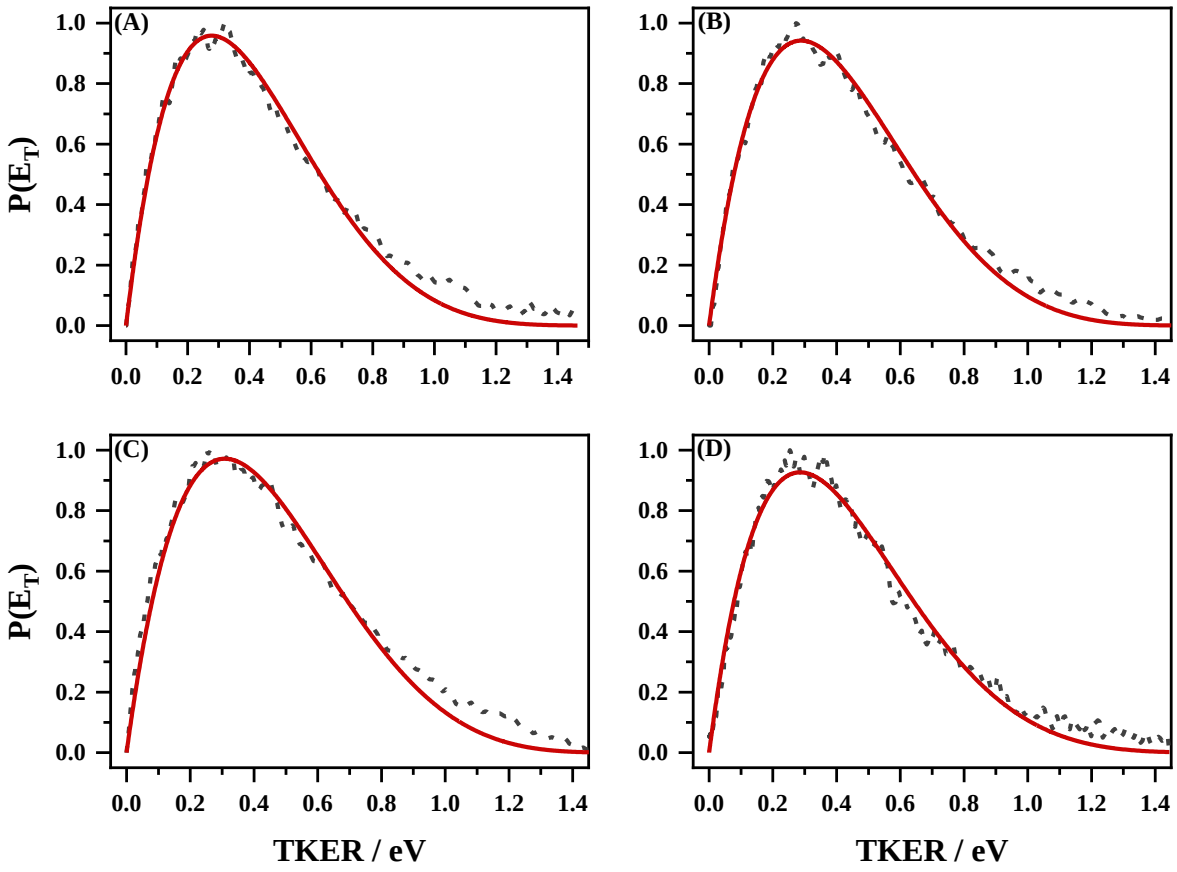

Figure 4. Normalized TKER distribution profiles of the methyl fragment originating from (A) *o*-xylene, (B) *m*-xylene, (C) *p*-xylene and (D) mesitylene. In each panel the dashed black trace represents the experimental TKER, and the solid red curve represents the fit based on the empirical fitting function shown in equation 2. For *o*-xylene (b =4.87; R^2=0.988), *m*-xylene (b=4.61; R^2=0.990), *p*-xylene (b=4.32; R^2=0.992), and mesitylene (b ~~a~~=5.20; R^2=0.984) the value of E_T^{max} was fixed at 1.63, 1.62, 1.64 and 1.77 eV, respectively (see Table 2).

Further, the TKER distribution profiles of the methyl fragments were fitted to an empirical function given by equation (2).[37–39]

$$P(E_T) = C \cdot (E_T)^a \cdot (E_T^{max} - E_T)^b \qquad (2)$$

where $[P(E_T)]$ is the translational energy distribution function, 'a', 'b' are adjustable parameters, while 'C' is a normalization constant and E_T^{max} is the maximum translational energy available for the fragments in the center-of-mass frame after dissociation. However, it must be pointed out that E_T^{max} also includes the electron kinetic energy after ionization, therefore E_T^{max} is the sum of kinetic energies of the electron and the mass fragments. Fits to the TKER distribution profiles of the methyl fragment with equation 2 by fixing the E_T^{max} value (calculated by equation 1, see Table 2) resulted in a value of 'a' in the range of 0.9 – 1.1. Therefore, global analysis was performed by fixing the value of 'a' as 1in equation (2). Figure 4 shows the fitting of the empirical function (equation 2) to the TKER distribution profiles for all four cases, the agreement between the experimental data and the fits are excellent. It is known that a=1 in equation (2) indicates non-statistical TKER distribution.[39] Moreover, deviations on the higher kinetic energy side, originating due to multiphoton detection of the methyl radical, which appear to be only marginal in the present case, have been neglected.[39] Interestingly, the value of 'b' (from equation 2) are very similar for all the three isomers of xylene (4.87, 4.61 and 4.32 for ortho, meta and para isomers, respectively) and moderately different from mesitylene (5.20), which suggests that overall dynamics of methyl radical formation is insensitive to the position of substitution in xylenes but marginally dependent on the number of methyl groups.

CONCLUSIONS

Photodissociation of methyl benzenes viz., *o*-xylene, *m*-xylene, *p*-xylene, and mesitylene at 266 nm was investigated by probing the {sp^2}C–C{sp^3} dissociation channel leading to the formation of methyl fragment using velocity map imaging technique. The methyl radical in the ground (v=0) state was detected using a 2+1 REMPI scheme using a 333.45 nm laser. The images of the methyl fragment and the co-fragment were isotropic which suggests that the

dissociation timescale is slower than rotational reorientation time. The KER distribution profiles for the methyl radical were almost identical for all the three isomers of xylene and mesitylene. On the other hand, the KER distribution profiles for the co-fragment due to loss of one methyl group are different for *o*-xylene and *p*-xylene in comparison with *m*-xylene and mesitylene. Further, in the case of *o*-xylene, the TKER distribution curves for the methyl radical and the co-fragment are almost identical and have marginal differences in the case of *p*-xylene. However, significant differences were observed in the corresponding TKER distribution curves of *m*-xylene and mesitylene, which is attributed to the formation of the methyl radical from alternate channels. The TKER distribution profiles are rationalized based on {sp^2}C–C{sp^3} dissociation in the cationic state following a resonant [1+1+1] 3-photon process, due to lowering of the {sp^2}C–C{sp^3} bond dissociation energy relative to the neutral ground state. Based on the analysis of TKER distribution profiles of the methyl fragment using an empirical function, it was inferred that the dynamics of {sp^2}C–C{sp^3} bond dissociation is insensitive to the position of substitution in dimethyl benzenes (xylenes), but marginally dependent on the number of methyl groups.

ACKNOWLEDGMENTS

This study is based upon a work supported in part by the Science and Engineering Research Board of the Department of Science and Technology (Grant No. EMR/2016/000362) and Board of Research in Nuclear Sciences (BRNS Grant No. 58/14/18/2020) to GNP. NBB and SS thank CSIR India and DST-INSPIRE, respectively, for the research fellowship. MK is supported by the Women Scientists Scheme of the Department of Science and Technology (Grant No. SR/WOS-A/CS-18/2019).

REFERENCES

(1) Tsai, S. T.; Lin, C. K.; Lee, Y. T.; Ni, C. K. Dissociation Rate of Hot Benzene. *J. Chem. Phys.* **2000**, *113*, 67–70.

(2) Yokoyama, A.; Zhao, X.; Hintsa, E. J.; Continetti, R. E.; Lee, Y. T. Molecular Beam Studies of the Photodissociation of Benzene at 193 and 248 Nm. *J. Chem. Phys.* **1990**, *92*, 4222–4233.

(3) Ni, C. K.; Tseng, C. M.; Lin, M. F.; Dyakov, Y. A. Photodissociation Dynamics of Small Aromatic Molecules Studied by Multimass Ion Imaging. *J. Phys. Chem. B* **2007**, *111*, 12631–12642.

(4) Tseng, C. M.; Dyakov, Y. A.; Huang, C. L.; Mebel, A. M.; Lin, S. H.; Lee, Y. T.; Ni, C. K. Photoisomerization and Photodissociation of Aniline and 4-Methylpyridine. *J. Am. Chem. Soc.* **2004**, *126*, 8760–8768.

(5) Lin, M. F.; Lee, Y. T.; Ni, C. K.; Xu, S.; Lin, M. C. Photodissociation Dynamics of Nitrobenzene and O-Nitrotoluene. *J. Chem. Phys.* **2007**, *126*, 064310.

(6) Tseng, C. M.; Lee, Y. T.; Ni, C. K.; Chang, J. L. Photodissociation Dynamics of the Chromophores of the Amino Acid Tyrosine: P-Methylphenol, p-Ethylphenol, and p(2-Aminoethyl)Phenol. *J. Phys. Chem. A* **2007**, *111*, 6674–6678.

(7) Bounaceur, R.; Da Costa, I.; Fournet, R.; Billaud, F.; Battin-Leclerc, F. Experimental and Modeling Study of the Oxidation of Toluene. *Int. J. Chem. Kinet.* **2005**, *37*, 25–49.

(8) Battin-Leclerc, F.; Bounaceur, R.; Belmekki, N.; Glaude, P. A. Experimental and Modeling Study of the Oxidation of Xylenes. *Int. J. Chem. Kinet.* **2006**, *38*, 284–302.

(9) Adachi, S.; Suzuki, T. Methyl Substitution Effects on the Non-Adiabatic Dynamics of Benzene: Lifting Three-State Quasi-Degeneracy at Conical Intersections. *Phys. Chem. Chem. Phys.* **2020**, *22*, 2814–2818.

(10) Bolovinos, A.; Philis, J.; Pantos, E.; Tsekeris, P.; Andritsopoulos, G. The Methylbenzenes Vis-à-Vis Benzene. *J. Mol. Spectrosc.* **1982**, *94*, 55–68.

(11) Kovács, T.; Blitz, M. A.; Seakins, P. W.; Pilling, M. J. H Atom Formation from Benzene and Toluene Photoexcitation at 248 Nm. *J. Chem. Phys.* **2009**, *131*, 204304.

(12) Huang, C. L.; Jiang, J. C.; Lee, Y. T.; Ni, C. K. Photoisomerization and Photodissociation of M-Xylene in a Molecular Beam. *J. Phys. Chem. A* **2003**, *107*, 4019–4024.

(13) Park, J.; Bersohn, R.; Oref, I. Unimolecular Decomposition of Methylsubstituted Benzenes into Benzyl Radicals and Hydrogen Atoms. *J. Chem. Phys.* **1990**, *93*, 5700–5708.

(14) Zhou, Z.; Xie, M.; Wang, Z.; Qi, F. Determination of Absolute Photoionization Cross-Sections of Aromatics and Aromatic Derivatives. *Rapid Commun. Mass Spectrom.* **2009**, *23*, 3994–4002.

(15) Scott, T. W.; Braun, C. L.; Albrecht, A. C. Multiphoton Ionization in the Organic Condensed Phase: A Three-Photon Study of Liquid Benzene. *J. Chem. Phys.* **1981**, *76*, 5195–5202.

(16) Chen, C. H.; McCann, M. P. Measurements of Two-Photon Absorption Cross Sections for Liquid Benzene and Methyl Benzenes. *J. Chem. Phys.* **1988**, *88*, 4671–4677.

(17) Torma, K. G.; Voronova, K.; Sztáray, B.; Bodi, A. Dissociative Photoionization of the C 7 H 8 Isomers Cycloheptatriene and Toluene: Looking at Two Sides of the Same Coin Simultaneously. *J. Phys. Chem. A* **2019**, *123*, 3454–3463.

(18) Liu, Y.; Radi, P.; Gerber, T.; Knopp, G. Study on the Ultrafast Dynamics of O-Xylene Cation by Combined Fs-Photoelectron Imaging-Photofragmentation Spectroscopy. *Chem. Phys.* **2014**, *442*, 48–52.

(19) Liu, Y.; Yan, Y.; Yin, W.; Liu, B.; Gerber, T.; Knopp, G. Photoelectron Imaging

Spectroscopy and Photodynamics of M-Xylene Cations. *Laser Phys. Lett.* **2019**, *16*, 035301.

(20) Lin, C. K.; Huang, C. L.; Jiang, J. C.; Chang, A. H. H.; Lee, Y. T.; Lin, S. H.; Ni, C. K. Photoisomerization and Photodissociation of Toluene in Molecular Beam. *J. Am. Chem. Soc.* **2002**, *124*, 4068–4075.

(21) McMillen, D. F.; Golden, D. M. Hydrocarbon Bond Dissociation Energies. *Annu. Rev. Phys. Chem.* **1982**, *33*, 493–532.

(22) Held, A.; Selzle, H. L.; Schlag, E. W. Methyl Group Rotational Dynamics in O-, m-, and p-Xylene Cations from Pulsed Field Ionization Zero-Kinetic-Energy Spectroscopy. *J. Phys. Chem. A* **1998**, *102*, 9625–9630.

(23) Fujii, A.; Morita, S. I.; Miyazaki, M.; Ebata, T.; Mikami, N. A Molecular Cluster Study on Activated CH/π Interactions: Infrared Spectroscopy of Aromatic Molecule-Acetylene Clusters. *J. Phys. Chem. A* **2004**, *108*, 2652–2658.

(24) Mishra, S.; Bejoy, N. B.; Kawade, M.; Upadhyaya, H. P.; Patwari, G. N. Photodissociation of O-Xylene at 266 Nm: Imaging the CH3 Dissociation Channel. *J. Chem. Sci.* **2021**, *133*, 128.

(25) Suits, A. G. http://faculty.missouri.edu/suitsa/NuAqc.html.

(26) Schneider, C. A.; Rasband, W. S.; Eliceiri, K. W. NIH Image to ImageJ: 25 Years of Image Analysis. *Nat. Methods* **2012**, *9*, 671–675.

(27) Poullain, S. M.; Chicharro, D. V.; Rubio-Lago, L.; García-Vela, A.; Bañares, L. A Velocity-Map Imaging Study of Methyl Non-Resonant Multiphoton Ionization from the Photodissociation of CH3I in the A-Band. *Philos. Trans. R. Soc. A Math. Phys. Eng. Sci.* **2017**, *375*, 20160205.

(28) Hudgens, J. W.; DiGiuseppe, T. G.; Lin, M. C. Two Photon Resonance Enhanced Multiphoton Ionization Spectroscopy and State Assignments of the Methyl Radical. *J. Chem. Phys.* **1983**, *79*, 571–582.

(29) Lange, S.; Luther, K.; Rech, T.; Schmoltner, A. M.; Tree, J.; Chemie, P.; Gdttingen, U.; Gottingen, D.-. C-C and C-H Bond Splits of Laser-Excited Aromatic Molecules . 4 . Specific Rate Constants and Branching Ratios for the Dissociation of the Xylenes. *J. Phys. Chem.* **1994**, *98*, 6509–6513.

(30) Rittgers, B. M.; Leicht, D.; Duncan, M. A. Cation-ΠComplexes of Silver Studied with Photodissociation and Velocity-Map Imaging. *J. Phys. Chem. A* **2020**, *124*, 9166–9176.

(31) Vinklárek, I. S.; Rakovský, J.; Poterya, V.; Fárník, M. Clustering and Multiphoton Effects in Velocity Map Imaging of Methyl Chloride. *Mol. Phys.* **2021**, *119*, e1823507.

(32) Bain, M.; Hansen, C. S.; Ashfold, M. N. R. Communication: Multi-Mass Velocity Map Imaging Study of the Ultraviolet Photodissociation of Dimethyl Sulfide Using Single Photon Ionization and a PImMS2 Sensor. *J. Chem. Phys.* **2018**, *149*, 081103.

(33) Steglich, M.; Knopp, G.; Hemberger, P. How the Methyl Group Position Influences the Ultrafast Deactivation in Aromatic Radicals. *Phys. Chem. Chem. Phys.* **2019**, *21*, 581–588.

(34) Baboul, A. G.; Curtiss, L. A.; Redfern, P. C.; Raghavachari, K. Gaussian-3 Theory Using Density Functional Geometries and Zero-Point Energies. *J. Chem. Phys.* **1999**, *110*, 7650–7657.

(35) Frisch, M. J.; Trucks, G. W.; Schlegel, H. B.; Scuseria, G. E.; Robb, M. A.; Cheeseman, J. R.; Scalmani, G.; Barone, V.; Petersson, G. A.; Nakatsuji, H.; Li, X.; Caricato, M.; Marenich, A. V.; Bloino, J.; Janesko, B. G.; Gomperts, R.; Mennucci, B.; Hratchian, H. P.; Ortiz, J. V.; Izmaylov, A. F.; Sonnenberg, J. L.; Williams-Young, D.; Ding, F.; Lipparini, F.; Egidi, F.; Goings, J.; Peng, B.; Petrone, A.; Henderson, T.; Ranasinghe, D.; Zakrzewski, V. G.; Gao, J.; Rega, N.; Zheng, G.; Liang, W.; Hada, M.; Ehara, M.; Toyota, K.; Fukuda, R.; Hasegawa, J.; Ishida, M.; Nakajima, T.; Honda, Y.; Kitao, O.; Nakai, H.; Vreven, T.; Throssell, K.; Montgomery, J. A., J.; Peralta, J. E.; Ogliaro, F.; Bearpark, M. J.; Heyd, J. J.; Brothers, E. N.; Kudin, K. N.; Staroverov, V. N.; Keith, T. A.; Kobayashi, R.; Normand, J.; Raghavachari, K.; Rendell, A. P.; Burant, J. C.; Iyengar, S. S.; Tomasi, J.; Cossi, M.; Millam, J. M.; Klene, M.; Adamo, C.; Cammi, R.; Ochterski, J. W.; Martin, R. L.; Morokuma, K.; Farkas, O.; Foresman, J. B.; Fox, D. J. Gaussian 16, Revision B.01. Gaussian, Inc.: Wallingford CT 2016.

(36) Lias, Sharon G. Ausloos, P. Ionization Energies of Organic Compounds by Equilibrium Measurements. *J. Am. Chem. Soc.* **1978**, *100*, 6027–6034.

(37) Deyerl, H. J.; Fischer, I.; Chen, P. Photodissociation Dynamics of the Propargyl Radical. *J. Chem. Phys.* **1999**, *111*, 3441–3448.

(38) Pachner, K.; Steglich, M.; Hemberger, P.; Fischer, I. Photodissociation Dynamics of the Ortho - And Para -Xylyl Radicals. *J. Chem. Phys.* **2017**, *147*, 084303.

(39) Matthaei, C. T.; Mukhopadhyay, D. P.; Fischer, I. Photodissociation of Benzoyl Chloride: A Velocity Map Imaging Study Using VUV Detection of Chlorine Atoms. *J. Phys. Chem. A* **2021**, *125*, 2816–2825.